Journal of Biomechanics 46 (2013) 773–779

Contents lists available at SciVerse ScienceDirect

Journal of Biomechanics

journal homepage: www.elsevier.com/locate/jbiomech
www.JBiomech.com

Coupling between the spinal cord and cervical vertebral column under tensile loading

Shannon G. Kroeker*, Randal P. Ching

Applied Biomechanics Laboratory, Department of Mechanical Engineering, University of Washington, 501 Eastlake Ave E, Ste 102, Seattle, WA 98109, United States

ARTICLE INFO

Article history:
Accepted 9 November 2012

Keywords:
Cervical spine
Spinal cord
Primate model
Strain
Tension
Biomechanics
Neck

ABSTRACT

Current neck injury criteria are based on structural failure of the spinal (vertebral) column without consideration of injury to the spinal cord. Since one of the primary functions of the vertebral column is to protect the cord, it stands to reason that a more refined measure of neck injury threshold would be the onset of spinal cord injury (SCI). This study investigated the relationship between axial strains in the cervical vertebral column and the spinal cord using an *in vitro* primate model ($n=10$) under continuous tensile loading. Mean failure loads occurred at 1951.5 ± 396 N with failure strains in the vertebral column of $16 \pm 5\%$ at the level of failure. Average tensile strains in the spinal cord at failure were $11 \pm 5\%$ resulting in a mean coupling ratio of 0.54 ± 0.17 between C1 and C7. The level of peak strain measured in the spinal cord did not always occur at the location of vertebral column failure. Spinal cord strains were less than spine strains and coupling ratios were not significantly different along the length of the spine. The largest coupling ratio was measured in the atlanto–occipital joint whereas the smallest coupling ratio occurred at the adjacent C1–C2 joint.

1. Introduction

Spinal cord injury (SCI) results in detrimental loss of bodily functions. Motor vehicle collisions are the most prevalent cause for cervical SCI (The National SCI Statistical Center 2008). Sudden accelerations and decelerations of the head and body apply forces to the cervical vertebral column which can exceed the injury tolerance. Consequently, the vertebrae may be stretched apart and the loads transferred to the spinal cord. Damage occurs when this strain exceeds a threshold. In order to prevent SCIs, the mechanisms by which they occur must be better understood.

To study the risk of SCI, injurious scenarios are recreated using anthropomorphic test dummies in simulated car crashes, laboratory experiments, or computational models. To assess injury risk, each technique requires knowledge of the threshold forces, accelerations, and/or displacements that correlate to SCI. Currently, threshold values for cervical spine injury are based on structural failure of the bones and ligaments in the cervical column, excluding SCI (Eppinger et al., 1999). However, clinical cases of SCI demonstrate that structural failure of the vertebral column can happen after SCI, as occurs in SCIWORA for example (Gupta et al., 1999; Kokoska et al., 2001; Kothari et al., 2000; Martin et al., 2004). Because SCI occurs before structural failure of the vertebral column, the current threshold for injury ignores the potential for SCI which may have already occurred by the time the threshold for vertebral column injury is reached. In order to improve our understanding of cervical injury and incorporate measures for SCI into our definition of a cervical injury threshold, it is imperative that the relationship between vertebral column failure and SCI is better defined in terms of vertebral column strain or displacement.

The spinal cord is often difficult to incorporate into laboratory testing of the vertebral column since it does not retain its mechanical properties post-mortem. Accordingly, the effect of forces and displacements applied to the vertebral column is often not correlated with the onset of SCI. The coupling ratio, a ratio of spinal cord strain to vertebral column strain, provides a method to estimate the spinal cord strain in tests where the vertebral column strains are measured but the spinal cord is not incorporated. The vertebral column strain at the onset of SCI can then be used as a more clinically relevant tolerance for the spine as opposed to complete vertebral column failure.

This study focuses on the correlation between vertebral column and spinal cord strains as it relates to tension–extension injuries which occur in instances such as whiplash (Shea et al., 1992), airbag deployment beneath the chin (Eppinger et al., 2000; Klinich et al., 1996; NHTSA, 1999; Pintar et al., 2000; Stalnaker, 1993), frontal collisions (Panjabi and Myers, 1995), pilot ejection (Carter et al., 2000), and spinal surgery with traction (Yeoman

* Corresponding author. Tel.: +1 604 738 6728.
E-mail addresses: shannon.kroeker@gmail.com (S.G. Kroeker), rc@u.washington.edu (R.P. Ching).

0021-9290/$ - see front matter © 2012 Elsevier Ltd. All rights reserved.
http://dx.doi.org/10.1016/j.jbiomech.2012.11.012

et al., 1989). The objectives of this study were to determine, using a non-human primate (NHP) model, the coupling relationship between spinal cord and vertebral column strains, as the vertebral column is continuously distracted to complete column failure, to further elucidate the temporal nature of SCI and its relationship to vertebral column failure.

2. Methods

Cervical vertebral column testing was performed with ten cadaveric *Macaca nemestrina* (age = 14.8 ± 3.6 years, weight = 7.4 ± 1.2 kg). All animals were greater than eight years old to match the human equivalent adult age in cervical spine development (Fesmire and Luten, 1989; Kramer et al., 2002; Lamparski and Nanda, 2002; Minars et al., 2003; Ogden et al., 1994; Reilly, 2007). Experiments were completed within 4 h post-mortem to minimize the decomposition effect on neurologic and muscle tissue mechanical properties (Gefen and Margulies, 2004; Hung and Chang, 1981; Oakland et al., 2006; Van Ee et al., 2000a). Radiopaque markers were affixed to the vertebrae and spinal cord to enable fluoroscopic visualization and tracking. A high-definition video camera recorded continuous fluoroscopic images as the cervical spine was loaded to failure in tension–extension.

2.1. Specimen preparation

NHP specimens were obtained within 1 h post-mortem following euthanasia for other unrelated research studies not affecting the musculoskeletal system. A longitudinal slit was made to the right of the spinous processes from the occipital bone to T1. Lead beads (2 mm diameter) were affixed to the right vertebral laminae from C2–C7 and the right aspect of the posterior arch of C1 using cyanoacrylate glue (Super Glue Corporation, USA). A radiopaque marker (a mixture of Barium Sulfate ($BaSO_4$) and a highly viscous paste (Neutrogena Deep Clean Cream Cleanser, Neutrogena Corp, USA)) was injected into the spinal cord between each pair of cervical vertebrae from the cranium to T1 (approximately 3 mm diameter).

2.2. Experimental setup

Each animal was laid supine on a custom acrylic table equipped with fixtures to impart tensile cervical loads. The acrylic directly below the neck was 1.6 mm thick in order to maximize fluoroscopic image quality. A harness was wrapped around the neck, just below the maxilla. The harness was attached to a load cell which was connected to a retractable pneumatic piston (Fig. 1). Acrylic blocks above the shoulders held the torso stationary. A steel bar across the maxilla was used to initially position the head–neck in extension at 46° ± 6° (across all specimens) from the transverse plane, and this angle was maintained throughout tensile loading.

A fluoroscope (Series 9000, OEC Diasonics, USA) was used to image the spine and spinal cord throughout distraction of the neck. A high-definition video camera (HDR-SR7, Sony USA) recorded the motion of the vertebrae via the fluoroscope, at 30 Hz. The resulting images had a resolution of 0.2 mm/pixel.

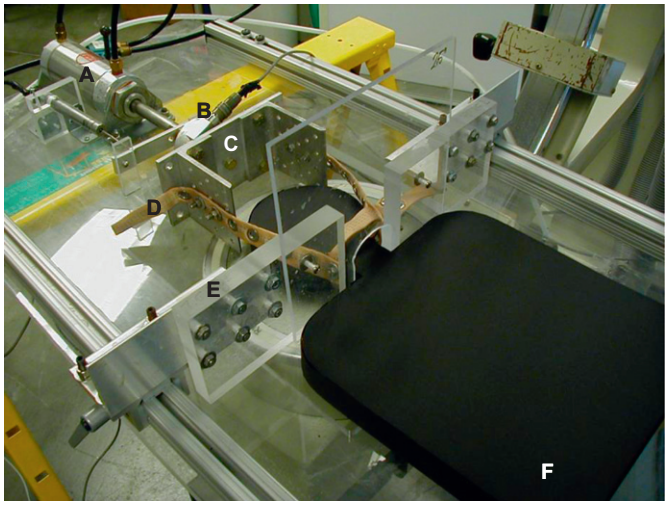

Fig. 1. Harness system. A—Pneumatic cylinder, B—load cell, C—aluminum C-frame, D—head restraint, E—shoulder restraint, F—specimen silhouette.

2.3. Instrumentation

Neck distraction was applied at 350 N/s over 5 s using a pneumatic cylinder (704-DXP, Bimba, USA) controlled by a voltage operated pneumatic control valve (QB3, Proportion Air, USA). Loads were measured using a 4448 N (1000 lb) load cell (262257, Sensotec, USA). Load data was amplified using a Vishay 2310 Signal Conditioning Amplifier (Vishay, USA). Data collection and device control were performed using LabView 7.0 (National Instruments, USA) and two data acquisition devices with voltage output capabilities (PMD 1208LS, Measurement Computing, USA).

2.4. Loading protocol

An initial pretension was applied to the neck, not exceeding 150 N, and one preconditioning cycle up to 300 N was performed to remove slack in the harness. The test commenced with a pretension of approximately 150 N.

2.5. Post-test analysis

The level of cervical spine failure was determined through post-injury inspection. Spinal cord transection levels were determined by fluoroscopic video analysis.

The fluoroscopic videos contained an inherent distortion. An image correction algorithm was determined by imaging a precision-machined square grid of lead beads, with an inter-bead distance of 12.7 mm (0.5″), to correct distortion and calibrate distances. Prior to calibration, the root mean square (rms) difference of the uncalibrated imaged grid relative to the actual grid was 2.91 ± 0.21 mm. Post calibration, the rms difference was reduced to 0.74 ± 0.06 mm.

A custom Matlab (R2008b, Mathworks USA) program was used to extract the marker location data throughout loading (Fig. 2). True strains were calculated separately for the vertebral column and the spinal cord. Of interest were the strains between the occiput (Occ) and C7 as well as between adjacent vertebrae from Occ to C7. Strains were analyzed up until vertebral column failure. Coupling ratios were calculated as the slope of the least-squares fit between spinal cord and vertebral column strain.

Displacement uncertainties were corrected using a spatio-temporal smoothing algorithm. A Kriging technique (Emadi et al., 2009; Orum et al., 1999) was used to estimate and refine the spatio-temporal location of each marker based on the positions of the other markers. This was repeated for each marker. The RMS difference between the smoothed and the raw marker positions was 0.42 ± 0.34 mm which verified that the smoothed data were not significantly altered from raw data.

3. Results

All experiments resulted in complete dislocation of the tissues between the vertebrae at a mean failure load of 1952.5 ± 396 N (Table 1). Failure most often occurred in the upper cervical spine between the Occ and C1 (70%). Peak strains in the vertebral column tended to occur between C1 and C2 (60%). Peak spinal cord strains varied between all experiments and spanned both the upper and lower cervical spine.

To investigate the cord–column coupling relationship, the vertebral column and spinal cord strains were plotted together (Fig. 3). From the onset of load application, vertebral columns strains exceeded spinal cord strains, and their difference increased as tension–extension loads increased. Column strains across the entire cervical spine (C1–C7) and between the Occ and C7 were also computed to describe the multi-segmental cervical spine strains of the cord and column.

The peak segmental strains in the vertebral column correlated with vertebral failure location ($p < 0.001$), as did peak segmental strains in the spinal cord ($p = 0.028$) (Fig. 4). Lower peak spinal cord and segmental vertebral column strains correlated with vertebral column failures near the occiput. A similar trend was not observed for the peak spinal cord strains and the level of cord transection.

To examine differences between the vertebral column and spinal cord strains, a coupling ratio was defined as the ratio of spinal cord strain to vertebral column strain. The coupling ratio describes the relationship between the stretch in the vertebral column and the spinal cord since they are not rigidly linked.